Chapter 74
Performance Improvement in a BIST Water Collector: A Parametric Study

Gilles Notton, Christian Cristofari, Fabrice Motte and Jean-Louis Canaletti

Abstract A flat-plate solar collector with high building integration was designed and prototyped. The experimentations showed that the performances of this solar collector can be improved. A numerical thermal model, developed in Matlab® environment using a finite difference model, was validated. Then, a modelling of the complete solar domestic hot water system (solar collector + water storage + piping) was realized. The performance of this system was calculated for various solar collector configurations such as the number and the position of the water pipes, air layer thickness, fluid flow rate, etc. Several solar fractions were used to implement this optimization procedure. An optimized solar collector structure is finally presented.

Keywords Thermal solar collector · Building integration · Modelling · Experimentation · Optimization

74.1 Introduction

A large Web survey on architectural integration of solar technologies (addressed to more than 170 European architects and building professionals) [1] showed that the architectural integration is a major issue in the development and spreading of solar thermal technologies.

First, we present the patented concept and the implemented experiment. Second, we underline the main negative points noted during the experiment. Third, we present the numerical models developed for each part of the thermal system: the first one for the solar collector presented in detail in [2] and a second one for the storage and the thermal loop inspired by the work of Haillot et al. [3]. This numerical model will be used for determining the best configuration of the thermal system and studying the influence of various parameters such as flow rate and air layer thickness. At last, we present a new improved configuration of the solar collector.

G. Notton (✉) · C. Cristofari · F. Motte · J.-L. Canaletti
Research Centre of Vignola, University of Corsica Pasquale Paoli, UMR CNRS 6134,
Centre of Vignola, Route des Sanguinaires, F20000 Ajaccio, France
e-mail: gilles.notton@univ-corse.fr

A. Sayigh (ed.), *Renewable Energy in the Service of Mankind Vol II,*
DOI 10.1007/978-3-319-18215-5_74

74.2 Solar Collector and Experiment

The patented concept H2OSS® is invisible from the ground because it is inserted within a drainpipe (Fig. 74.1) which conserves its rainwater evacuation role. The canalizations connecting the house to the heating collector are hidden in the vertical drainpipe. An installation consists of several connected modules. One module is about 1 m length and 0.1 m in width (individual houses), and larger modules can be developed for buildings. The number of modules depends on the drainpipe length. The structure of the collector is composed of glass, an air layer, a highly selective absorber, and an insulation layer (Fig. 74.1). The cold fluid flows from the tank through the inferior insulated tube and then into the upper tube in thermal contact with the absorber.

The experimentation (Fig. 74.3) allowing one to operate closer to the European Standard EN 12975-1 was implemented to test the thermal behaviour, to validate the thermal model, and to improve the performances by some parameter adjustments. Four rows of four thermal modules (1.8 m^2), connected in serial or parallel, are fixed to a solar tracker for better control of the solar intensity and direction (Fig. 74.2).

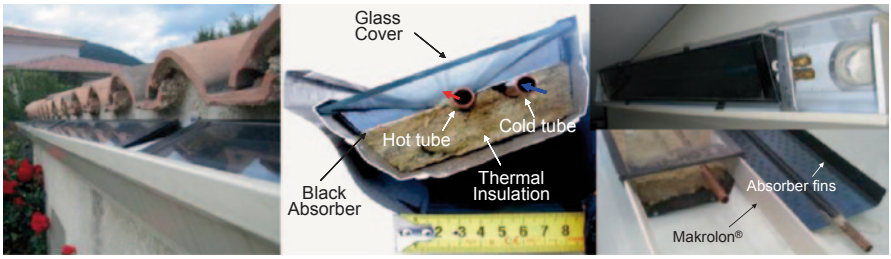

Fig. 74.1 The solar collector H2OSS®

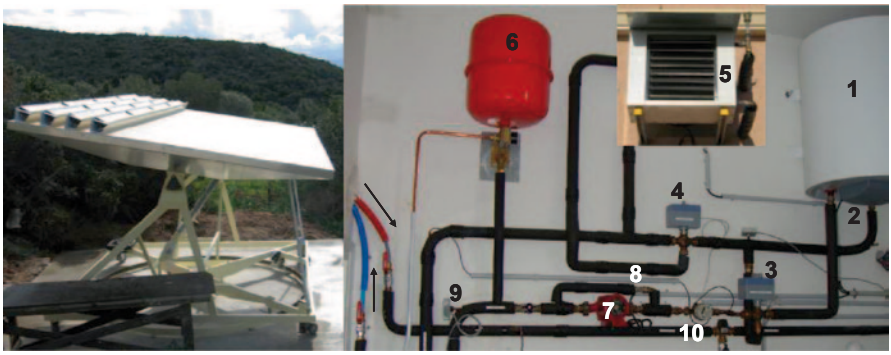

1. Water heater with electrical resistance 2.Temperature sensor (dry cooler gate control). 3. Water heater gate. 4. Dry cooler gate 5. Dry cooler (outdoor). 6. Expansion tank. 7. Pump. 8. Flow rate adjustment. 9. Temperature sensor (water heater gate control. 10. Flow meter

Fig. 74.2 The experiments: the solar tracker with H2OSS modules and the thermal loop

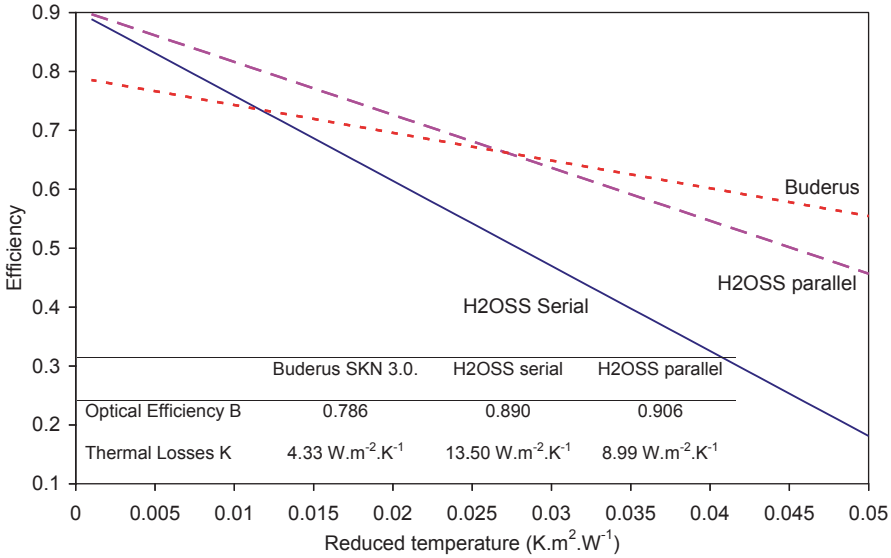

Fig. 74.3 Efficiencies versus the reduced temperature for H2OSS and Buderus SKN. 3.0

We compared the performances of the prototype with a commercial solar collector (Buderus 3.0) (Fig. 74.3); we calculated the optical efficiency and the thermal loss coefficient. Our optical efficiency is high, but the thermal losses are high particularly on the sides which are more important, and the performances decrease rapidly when the reduced temperature increases; the best performance is obtained with a low reduced temperature, that is with a low-input water temperature; it is more interesting to use a water storage tank with a thermal stratification, working at low flow rate with a colder temperature.

74.3 Thermal Models

The solar domestic hot water system is described in Fig. 74.4. The thermal model consists of 2 models:

- One for the H2OSS module, which calculates various temperatures in the solar collector [2]
- One for the hydraulic loop with water storage and distribution circuit developed by Haillot et al. [3]

We developed a bidimensional model with thermal transfers composed of a serial assembling of one-dimensional elementary models. The domain is broken up into elementary isotherm volumes, and for each of the 97 nodes, we write a thermal balance equation using an electrical analogy. All parameters of this model can be changed in such a way that we can estimate the influence of future changes on the

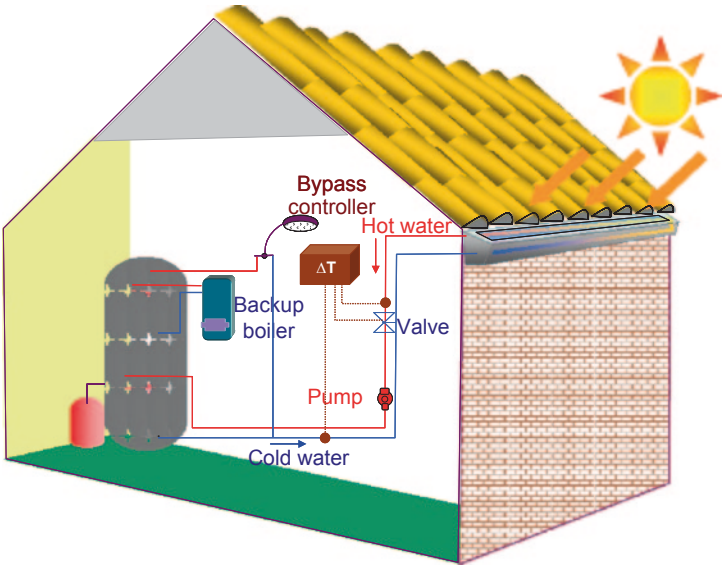

Fig. 74.4 The solar domestic hot water system

performances of solar module. The collectors can be connected in serial or parallel; in the first case, in the flow direction, the output fluid temperature of the first module becomes the input fluid temperature of the next one (Fig. 74.5); in the second case, the output temperature is the same for all the lines of modules and the total water flow rate is the sum of the flow rates of each line.

The experimental validation showed a good accuracy of the model: the relative root mean square errors are around 5 % for the water temperatures and from 4.6 to 10 % for the internal ones [2].

During the experimentation, the hydraulic resistance due to the linear structure was a problem. To reduce it, the solar system must work at low flow rate with these advantages [4]:

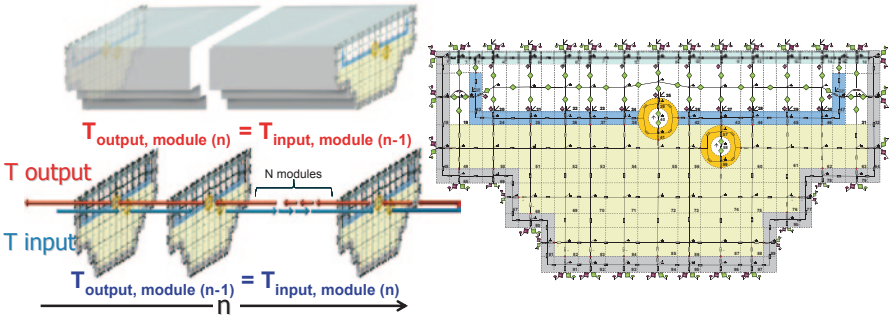

Fig. 74.5 Electrical analogy of the solar thermal collector and serial connexion

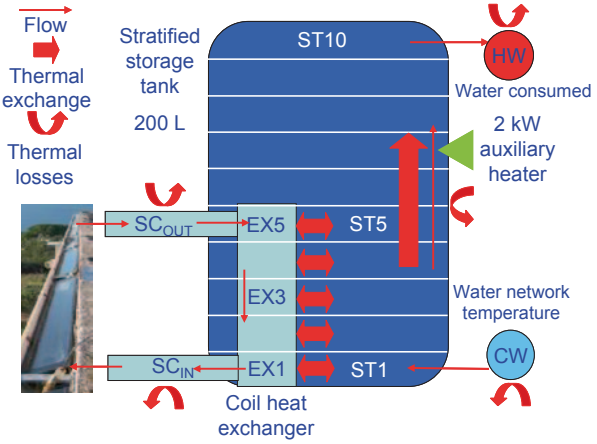

Fig. 74.6 Model node definitions [3]

- Thermal stratification: Using low flow operation results in an increased outlet temperature from the collector and a higher degree of thermal stratification inside the heat storage, the temperature at the top of the storage will be closer to the desired load temperature reducing the auxiliary energy consumption and increasing the solar fraction. The return temperature to the collector will be lowered, and the working periods and the output energy for the collector will be increased.
- Piping: We can use smaller pipes and the heat losses are reduced.
- Pump: The energy consumption of the pump is decreased which is very important in our case.

The thermal loop behaviour is simulated using a numerical code based on a nodal approach [3, 5]. It is divided into 19 nodes: 7 for the fluid circulation, 10 for the storage tank (optimal number of nodes for taking into account optimally the thermal stratification) [4], and 2 for the water inlet and outlet in the storage (Fig. 74.6). The temperature of water at the outlet of the solar collector and the average temperature of the solar absorber are obtained from the modelling of the solar collector.

The energy balance, in 1D, is applied and an iterative method is used to solve the first-order differential equations. A "reversion–elimination mixing algorithm" based on a thermal mix of some storage tank nodes to obtain a correction factor in order to have a positive temperature gradient from the bottom to the top of the tank [6, 7] is used to simulate the thermal stratification. More information on the water utilization profile and thermal regulation are given in [8].

The model of the thermal loop was validated by Haillot et al. [3] from measured data. The comparison between experimental and computed data is conduced to a relative root mean square error of 8.6% for the yearly average solar fraction; then, the thermal loop model is validated. We plotted in Fig. 74.7 the temperatures ST1–ST10 into the tank, and we see the stratification phenomenon. The two models have good accuracy and can be coupled to simulate the thermal behaviour of the total solar system.

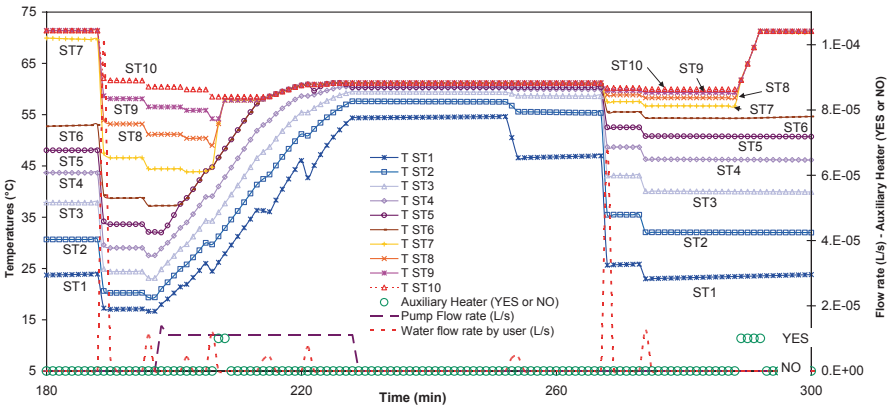

Fig. 74.7 Illustration of the thermal stratification into the storage tank

74.4 Solar Collector Optimization

To choose the optimal configuration, we calculate during each simulation the following data:

- The working time of the pump and its electrical energy consumed
- The working time of the electrical auxiliary heater and its electrical energy consumed
- The thermal energy drawn to the storage tank, that is useful for the user
- The thermal energy produced by the solar system (solar and electrical)
- The part of the thermal energy produced by the solar resource
- The thermal losses by the storage tank and the distribution water network

From these data, we defined three solar fractions:

- SF: the conventional solar fraction, which is the ratio of the total solar energy delivered to the tank $E_{\text{Thermal, Solar}}$ (kWh) and the total energy delivered to the tank E_{Thermal} (kWh). E_{Thermal} is the sum of the solar energy delivered to the tank and the auxiliary energy delivered to the tank.

$$SF = E_{\text{Thermal,solar}} / E_{\text{Thermal}} = E_{\text{Thermal,solar}} / \left(E_{\text{Thermal,solar}} + E_{\text{Electrical,AuxHeat}} \right). \quad (74.1)$$

- SF+: we noted that high hydraulic losses occur in the collector due to serial connexions. These losses impose the use of a high-power electrical pump with a high electrical consumption. It is necessary to take into account this supplementary energy due to the pump working in the solar fraction, and we added the electrical energy of the pump $E_{\text{Electrical,pump}}$ to the electrical energy used for the auxiliary heating:

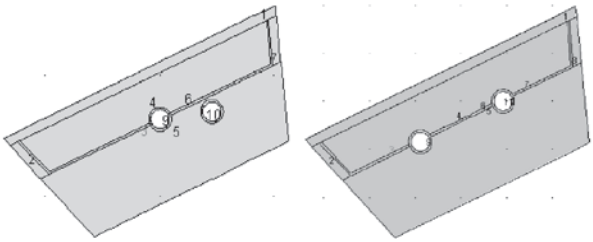

Fig. 74.8 The two versions of the solar collector H2OSS used for optimization

$$SF^{+} = E_{\text{Thermal,solar}} \Big/ \left(E_{\text{Thermal,solar}} + E_{\text{Electrical,AuxHeat}} + E_{\text{Electrical,pump}} \right). \quad (74.2)$$

- SF++: the value of electric power and thermal energy differs due to the form of energy. Electricity is a high-grade form of energy since it is converted generally from thermal energy. We used an overall thermal efficiency [9] $\eta_{\text{Ther-Elec}}$ for converting thermal energy into electricity and taken equal at 0.38. This formulation suggests energy equivalence between electricity and thermal energy with an electrical-to-thermal ratio equal to 2.63 (1/0.38):

$$SF^{++} = E_{\text{Thermal,solar}} \Big/ \left[E_{\text{Thermal,solar}} + \left(E_{\text{Electrical,AuxHeat}} + E_{\text{Electrical,pump}} \right) \Big/ \eta_{\text{Ther-Elec}} \right]. \quad (74.3)$$

We saw during the experiment that our collector has high heat losses due to its particular shape. The objective being to reduce the temperature of the absorber, we tested, after preliminary studies, a new configuration of the H2OSS collector called new version (Fig. 74.8).

Our optimization was realized for a solar system used by four persons in Corsica and composed by 35 serial connected modules (4 m^2) and a tank of 200 L. First, we verified that using 35 serial modules does not produce a temperature saturation, that is the water temperature continues to increase. Figure 74.9 shows, in steady state, the water temperature versus the number of modules (solar irradiance 750 W m^{-2}, ambient temperature 25 °C, wind speed 1 m s^{-1}, flow rate 60 L h^{-1}) for the two versions of solar collectors.

A more rapid saturation occurs for the new version but we can install efficiently, in serial order, 50 modules (50 m of gutter rarely available in a house). We used a pump with electrical power proportional to the flow rate between 30 W for 15 L h^{-1} and 250 W for 200 L h^{-1}. The calculations were realized for winter (January) and summer (July). We varied the fluid flow rate, the air thickness between cover and absorber (reduction in convective losses by the front face), and the insulation thickness (back and lateral thermal losses). The collector dimensions must stay within the commercial standards (the gutter must evacuate rainwater: limits of insulation). As an example, we show in Table 74.1, the monthly energies for the "current" configuration.

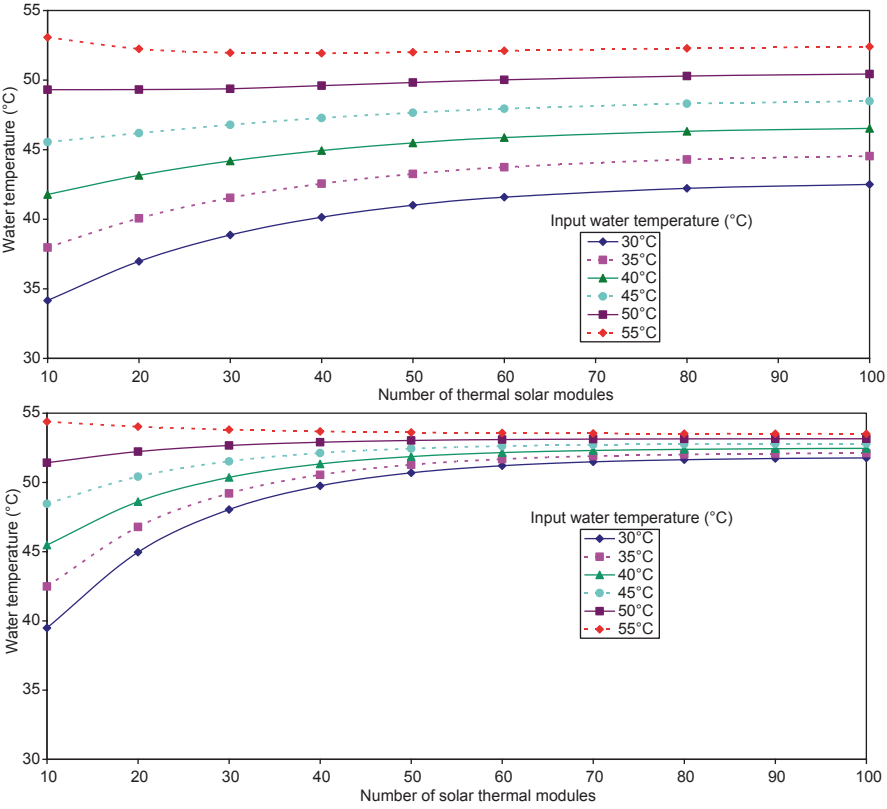

Fig. 74.9 Water temperature versus number of modules for current and new version of solar collector

Influence of the Flow Rate A low flow rate allows a thermal stratification of the storage, a hydraulic losses reduction, and a small pump power and tube diameter [10]. Hollands and Lightstone [11] calculated an annual energy gain of 38 % compared with high flow rate and Cristofari et al. [4] of 5.25 %. The hydraulic losses are high, and the fact to take into account is that the pump consumption in FR+ and FR++ should modify the optimization results compared with the use of FR. We see in Fig. 74.10 that the performances of the new version are better. Then, from now, we will only consider the new version. An optimum flow rate appears with SF+ and SF++ because they are a better indication of the performance level. The optimal flow rates are, respectively, 50 L h^{-1} and 75 L h^{-1} for summer and winter for the new configuration, and around 75 L h^{-1} for the current one. For winter, the performance gaps between a flow rate of 50 L h^{-1} and 75 L h^{-1} is lower than that in summer; thus, the optimum flow rate is taken equal to 50 L h^{-1} and the following optimization calculations will be realized for this flow rate, which is considered as a low flow rate; in fact, we consider as a low flow rate, a value between 7 and 15 L h^{-1} m^{-2} [12], that is for our 4 m^2 between 28 and 60 L h^{-1}.

Table 74.1 Example of calculation of the solar fractions for the current configuration

		January	July
Thermal energy drawn to the storage tank	kWh	182.3	171.0
Thermal losses (storage tank and water distribution circuit)	kWh	27.8	43.9
Thermal energy needs	kWh	210.1	215.0
Thermal energy produced by the solar resource	kWh	51.1	146.0
Running time of the pump	hour	62.5	21.9
Electrical energy for the pump	kWh	6.2	21.9
Running time of the auxiliary electric heater	hour	79	34.5
Electrical consumption of the auxiliary heater	kWh	159	69
Solar fraction SF	%	24.3	68
Solar fraction SF+	%	23.6	61.7
Solar fraction SF++	%	18.6	38.0

Influence of Air Thickness We calculated the three solar fractions for various air thicknesses (Fig. 74.11). The form of the curve is due to the variation of the convective coefficient in the air layer thickness. It appears in two optimums: 1 cm for winter and 1.125 cm for summer. The optimum is the same whatever the solar fraction used because the pump consumption has small influence. We chose an optimal value of 1.125 cm of air thickness. This result is in accordance with the literature [13] (Fig. 74.10).

Influence of Thermal Insulation We first studied the backside insulation but with the influence being small, the results will not be shown here. The very hot absorbers fins are insulated from the aluminium body by only 2 mm of Makrolon® (polycarbonate product). We added insulation between fins and body without decreasing the collection for thicknesses up to 16 mm for each side, but the maximum usable thickness is 4 mm for a gutter with good rainwater evacuation (Fig. 74.12).

From a thickness of 4–5 mm, the curves tend towards an asymptote. With an insulation of 4 mm on both sides (2 mm more than now), we have an improvement of 1.3 % in winter and 2 % in summer for SF.

74.5 Synthesis and Conclusion

From the previous results, we created an "ideal" H2OSS® solar collector with the characteristics summarized in Table 74.2 for a solar installation for four persons, situated in Corsica and 35 m of solar modules (4 m^2) for water storage of 200 L. To see the consequences of this optimization on the thermal performances, we plotted the efficiency versus the reduced temperature for the current and the new

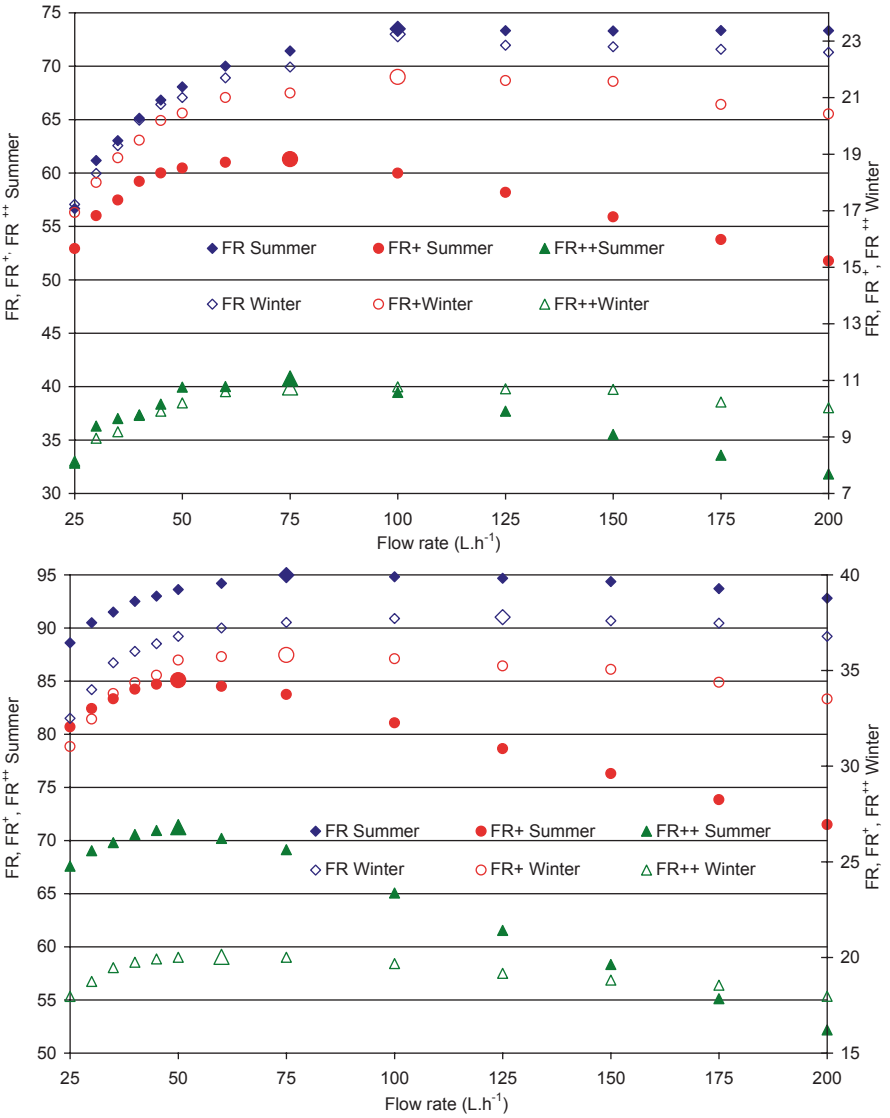

Fig. 74.10 Solar fractions versus water flow rate for the current and new version of the solar collector

optimized version in Fig. 74.13. The thermal loss coefficient decreases from 13.80 to 6.25 W m^{-2} K^{-1} (more than 50 %) but the optical coefficient decreases from 0.903 to 0.780 (−13 %). Despite the improvement of the thermal loss coefficient, it stays higher than that of the Buderus 3.0. (4.3 W m^{-2} K^{-1}) (Fig. 74.13).

The new positioning of the cold tube in the absorber and the optimization showed much better performance than with the actual prototype with an annual fraction passing from 41 % for the current version to 76 % for the new one.

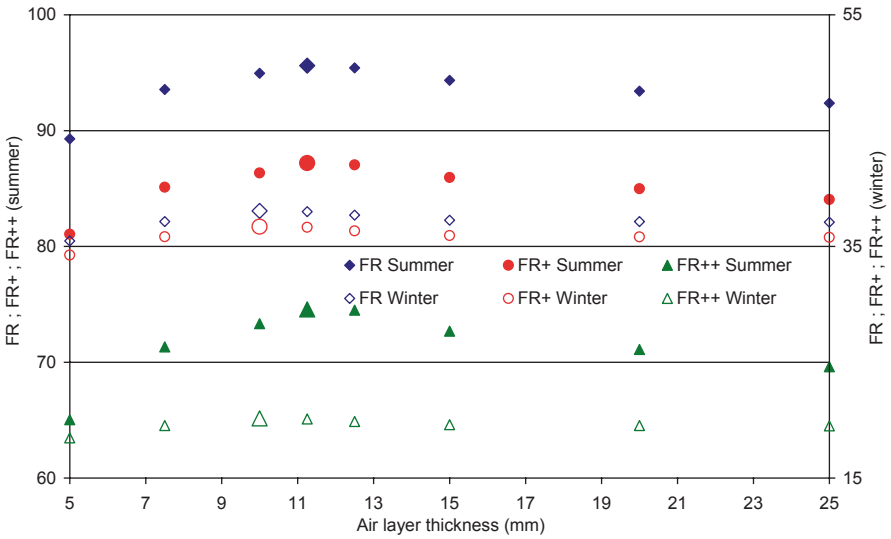

Fig. 74.11 SF, SF+, and SF++ versus the air layer thickness

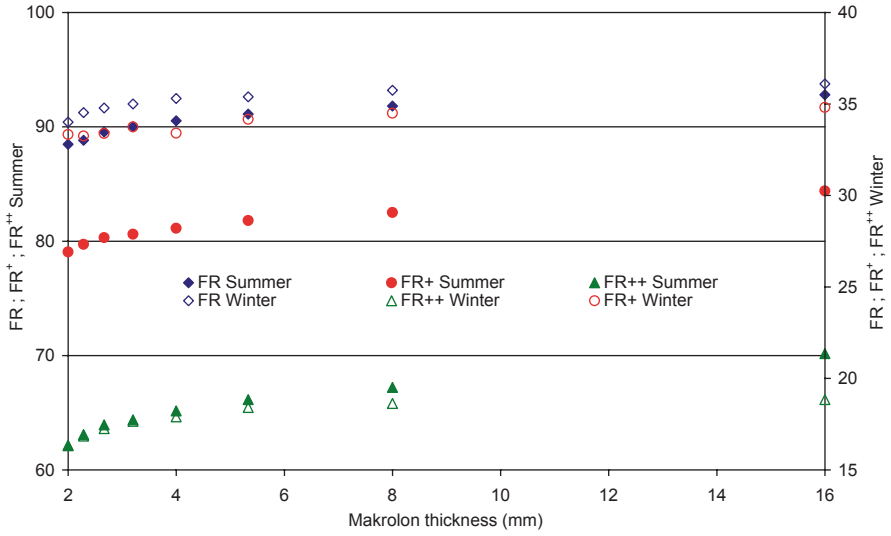

Fig. 74.12 Influence of the Makrolon® thickness between the absorber fins and the aluminium body

Table 74.2 Synthesis of the main optimization results

Parameter	Optimal value
Water tube positions	In the absorber (the cold tube is no longer in the insulation)
Flow rate	50 L h^{-1}
Air layer thickness	1.125 cm
Backside thermal	No more
Makrolon® insulation	+2 mm on both sides

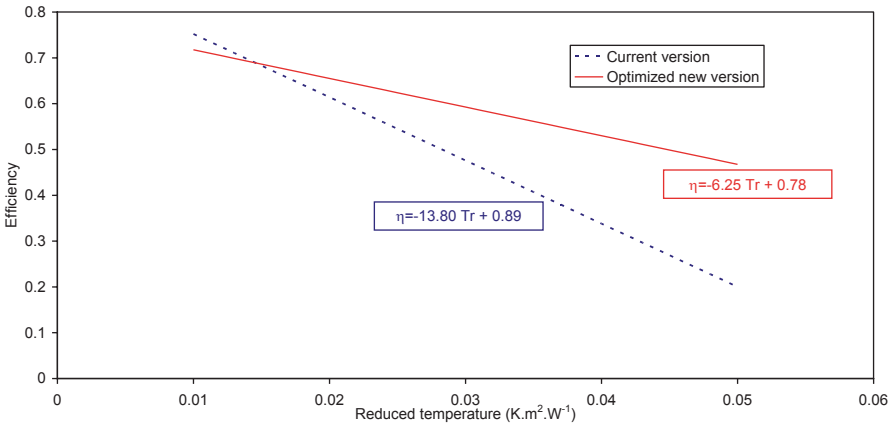

Fig. 74.13 Performance straight lines for current and optimized versions

Acknowledgements The authors thank the Territorial Collectivity of Corsica and OSEO-ANVAR for their financial supports. This work was realized in the frame of the COST Action TU1205 on "Building Integration of Thermal Solar Systems (BISTS)".

References

1. Munari Probst MC, Roecker C (2007) Towards an improved architectural quality of building integrated solar thermal systems (BIST). Sol Energy 81:1104–1116
2. Motte F, Notton G, Cristofari C, Canaletti JL (2013) Design and modelling of a new patented thermal solar collector with high building integration. Appl Energy 102:631–639
3. Haillot D, Nepveu F, Goetz V, Py X, Benabdelkarim M (2012) High performance storage composite for the enhancement of solar domestic hot water systems Part 2: numerical system analysis. Solar Energy 86(1):64–77
4. Cristofari C, Notton G, Poggi P, Louche A (2003) Influence of the flow rate and the tank stratification degree on the performances of a solar flat-plate collector. Int J of Thermal Sci 42(5):455–469
5. Haillot D (2009) Matériaux composites à hautes performances énergétiques pour l'optimisation des chauffe-eau solaires individuels: du matériau au procédé, Phd dissertation, University of Perpignan, France, (in French)

6. Mather D, Hollands KG, Wright J (2002) Single- and multi-tank energy storage for solar heating systems: fundamentals. Sol Energy 73:3–13
7. Nepveu F (2008) Production décentralisée d'électricité et de chaleur par système Parabole/Stirling: Application au système EURODISH, Phd dissertation, University of Perpignan
8. Notton G, Motte F, Cristofari C, Canaletti JL (2014) Performances and numerical optimization of a novel thermal solar collector for residential building. Ren Sust Energy Rev 33:60–73
9. Huang BJ, Lin TH, Hung WC, Sun FS (2001) Performance evaluation of solar photovoltaic/thermal systems. Sol Energy 70:443–448
10. Shah LJ (1999) Investigation and modeling of thermal conditions in low flow SDHW systems, Department of Buildings and energy Technical University of Denmark Report R-034
11. Hollands KGT, Lightstone MF (1989) A review of low flow, stratified-tank solar water heating systems. Sol Energy 43(2):97–105
12. Kenjo L, Inard C, Caccavelli D (2007) Experimental and numerical study of thermal stratification in a mantle tank of a solar domestic hot water system. Appl Therm Eng 11–12:1986–1995
13. Ferahta FZ, Bougoul S, Ababsa D, Abid C (2011) Numerical study of the convection in the air gap of a solar collector. Energy Procedia 6:177–185